Pressure effects on the electronic properties of PrAg in the ferromagnetic phase

1996 J. Phys.: Condens. Matter 8 10457

(http://iopscience.iop.org/0953-8984/8/49/033)

J. Phys.: Condens. Matter **8** (1996) 10457–10466. Printed in the UK

Pressure effects on the electronic properties of PrAg in the ferromagnetic phase

P K Sinharoy†, S K De‡ and S Chatterjee‡

† Department of Physics, Serampore College, District-Hooghly, Pin.-712201, West Bengal, India
‡ Department of Materials Science, Indian Association for the Cultivation of Science, Calcutta 700032, India

Received 24 April 1996, in final form 27 August 1996

Abstract. The electronic structure of PrAg in the ferromagnetic phase has been studied as a function of pressure. The magnetic instability is analysed by calculating the total energy in the local density approximation. From the spin-polarized calculation, it is found that the magnetic moment decreases under pressure. The constant f occupation number as a function of pressure indicates that the moment reduction is not due to the f electrons' delocalization.

1. Introduction

The pressure-induced structural and magnetic phase transitions of the Ag-based light rare earth, RAg (R = Ce, Pr, Nd), intermetallic compounds are interesting phenomena [1–13]. All the compounds exhibit a cubic-to-tetragonal structural phase transition at high pressure and low-temperature. The critical pressure at which such a transition occurs increases as one moves from Ce to Nd and it is explained on the basis of the band Jahn–Teller model [14]. The magnetic structure and its phase transition with the application of pressure (6–30 kbar) [10] are quite different for all these compounds. CeAg is ferromagnetic (FM), PrAg is both antiferromagnetic (AFM) and ferromagnetic and NdAg is antiferromagnetic at high pressure and low temperature. The various anomalous properties in the magnetic ground state, such as a low ferromagnetic transition temperature and a low saturation magnetic moment are observed under pressure [15]. The magnetic ground state of many intermetallic Ce compounds is unstable under pressure. The origin of this instability may be interpreted in terms of competition [16–18] between Ruderman–Kittel–Kasuya–Yosida (RKKY) interaction [19] and the Kondo effect [20].

The intermetallic compound PrAg, among all the light RAg compounds, is interesting because it exhibits intriguing magnetic properties at low temperature and high pressure. Several experiments by resistivity [9, 11], magnetization [10] and neutron diffraction measurement [6, 7] on its magnetic properties have established that (i) the spin structure is antiferromagnetic (AFM) below the Néel temperature $T_N \simeq 11$ K and can be changed into a canted spin structure with a magnetic field and (ii) the ferromagnetic (FM) component appears below the Curie temperature $T_C \simeq 6.9$ K and there is a sharp jump in the magnetization at high magnetic field. The AFM ($\pi\pi 0$) structure consists of FM (110) planes coupled antiferromagnetically. The noticeable point is that most RAg compounds are AFM with ($\pi\pi 0$) structure except for CeAg which is FM. Thus PrAg lies at the boundary between the domains of stability of the FM and AFM phases. The magnetic properties

0953-8984/96/4910457+10$19.50

of PrAg are interpreted in terms of the biquadratic exchange interaction [7] and the s–f exchange model [21]. In the first model, the total exchange energy consists of two parts: (i) bilinear exchange energy which favours ($\pi\pi 0$) type collinear AFM ordering and (ii) negative biquadratic exchange energy which favours quadrature spin ordering. Brun *et al* [6] first suggested that the competition between two such exchange energies could bring about the peculiar magnetic structure of PrAg. The magnetic behaviour at high pressure can be explained in terms of the indirect exchange interaction between the localized f and 5d6s band electrons, namely the s–f exchange model.

The pressure–temperature magnetic and structural phase diagrams of PrAg are complicated [8]. The cubic-to-tetragonal phase transition occurs at the critical pressure $P_c = 10$ kbar at a temperature of 13 K. In the cubic phase the values of T_N are almost pressure-independent whereas that of T_C increases rapidly with increasing pressure and equals T_N near 5 kbar. In the tetragonal phase T_C decreases drastically but T_N decreases slightly with increasing pressure. The large decrease in T_C indicates the instability of the ground state FM phase under pressure. This stimulated us to study the FM phase at different pressures. The magnetic properties of PrAg may be characterized by the RKKY–Kondo interaction, as found in most metallic Ce compounds. Both effects are determined by the hybridization of the localized f states with the extended states and also the density of states at the Fermi energy. Therefore, a detailed study of the electronic structure of PrAg is of paramount importance.

Our main aim in this paper is to study the electronic structure at high pressure and to ascertain the main mechanism that drives the magnetic properties of PrAg. Since the structural and the magnetic phase transition occur at different pressures and temperatures, we have studied ferromagnetic properties for a fixed structure, namely cubic CsCl, as a function of pressure by spin-polarized electronic structure calculations. This assumption gives almost the same results as does that of the tetragonal structure, since the tetragonal distortions from the cubic CsCl structure are quite small. We have also performed calculations with the reduced lattice constants shown in table 1, in order to reproduce the effect of an applied hydrostatic pressure.

Table 1. Input parameters for LMTO calculations. a are lattice constants, R_{WS} are Wigner–Seitz radii and E_F is the Fermi energy.

a (au)	R_{WS} (Pr) (au)	R_{WS} (Ag) (au)	E_F (Ryd)
$a_1 = 6.614$	3.452	3.034	0.617
$a_2 = 6.709$	3.501	3.078	0.577
$a_3 = 6.803$	3.557	3.113	0.545
$a_4 = 6.897$	3.607	3.156	0.514
$a_5 = 7.026$	3.682	3.203	0.476

We have, however, ignored the spin–orbit interactions because the treatment of f states in magnetic system is a difficult task since, in a fully relativistic formalism, spin is no longer a good quantum number [22], making the interpretation much more difficult. We have also neglected the tetragonal distortion because this would only bring about band splitting similar to the spin–orbit interaction. We hope that this will not disturb the trends in the picture of the electronic structure.

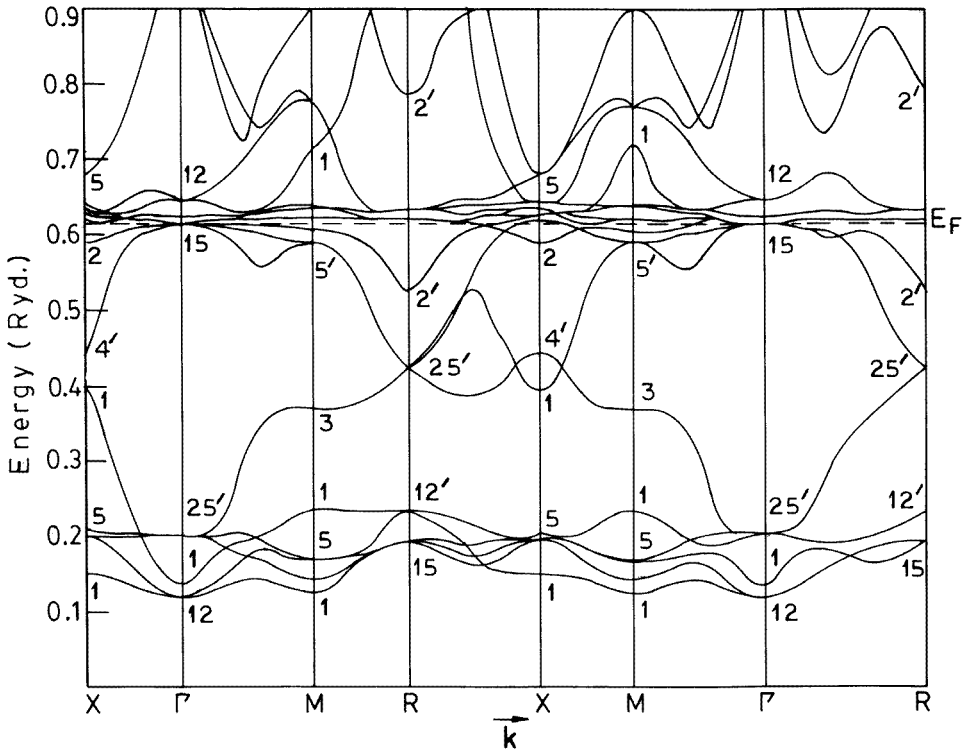

Figure 1. The band structure for the majority of spin at high pressure along the major symmetry axes in the Brillouin zone. E_F is the Fermi energy.

2. Calculational details

The band structure calculations were performed using the self-consistent linear muffin-tin orbital method [23, 24] in the local spin density approximation (LSDA) for the construction of the crystal potential. The LSDA of von Barth and Hedin [25] was used to represent the exchange and correlation potential. The initial potential was constructed from atomic Pr and Ag with the external configurations $4f^2 5d^2 6s^1$ and $4d^{10} 5s^1$ respectively. These outer electrons are treated as valence electrons whereas the inner electrons except for the p states of Pr are treated as core electrons during the iterations. The p states of Pr are treated as semi-core states during the iterations. The full Dirac equation was employed for the core states while the band electrons were treated semi-relativistically without the inclusion of the spin–orbit interactions. Lattice constants and the Wigner–Seitz radii used in this calculation are given in table 1. The density of states (DOS) was calculated by the tetrahedron method [26].

3. Results and discussion

The calculated band structures for the majority and minority spins at high pressure along the major symmetry axes in the Brillouin zone (BZ) are shown in figures 1 and 2 respectively. The band structure consists of occupied d and s bands of Ag and s bands of Pr, plus partially occupied f and unoccupied d bands of Pr. The narrow d bands of Ag are completely

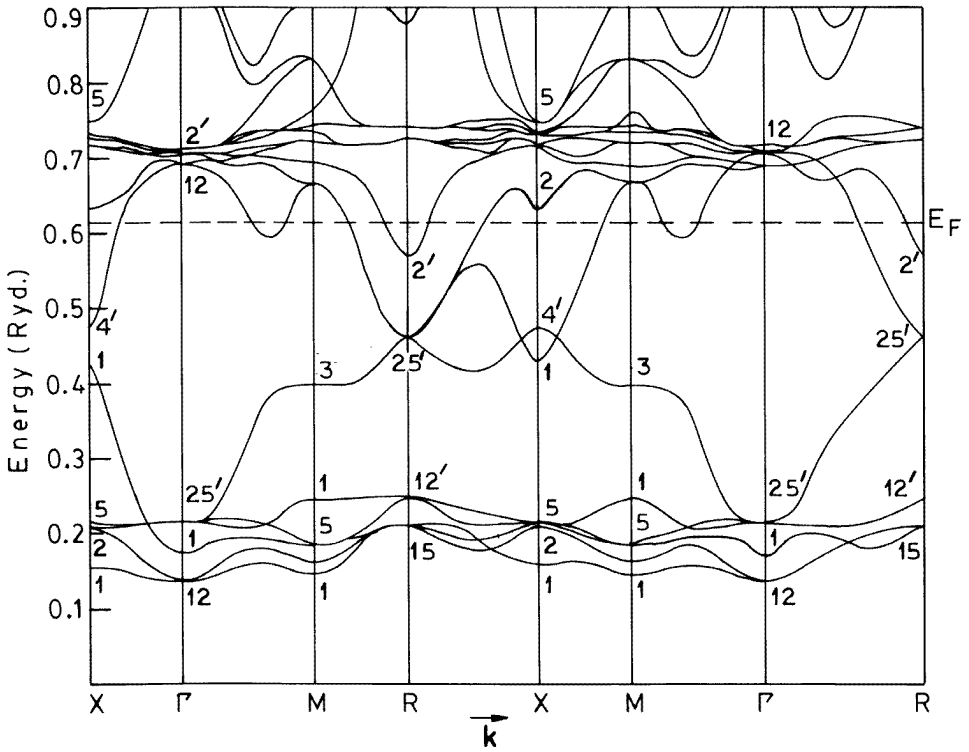

Figure 2. The band structure for the minority of spin at high pressure along the major symmetry axes in the Brillouin zone. E_F is the Fermi energy.

separated from the f bands of Pr. Thus there is no direct overlap between the d (Ag) and f (Pr) bands. The s and d bands of Pr are broad bands. The f bands are therefore immersed within a sea of electrons in the s–d conduction bands.

The behaviour of the eigenvalues under pressure for both spins at the Γ and X points is shown in figure 3. The states Γ_{12} and Γ'_{25} of the d band (Ag) and the Γ_1 state of the s band lie well below E_F and move downwards with reduction of volume for both spins. The states for the majority spin near E_F do not change appreciably with the application of pressure. The sensitive states near E_F at high pressure for the minority spin are Γ'_2 and Γ_{15}, originating from Pr f states, which rise, whereas the state Γ_{12} from Pr d states decreases in energy relative to E_F. Thus Γ_{12} is the lowest state for the minority spin while Γ_{15} is the lowest state for the majority spin above E_F. From figure 3 it can be observed that the f band rises in energy relative to the conduction d band for the minority spin. The states at the X point originating from the d states of Ag move downwards with pressure. The gap between X_1 and X'_4 states increases slightly with pressure.

Figures 4 and 5 show the total and partial density of states (DOS) respectively for both spins at ambient and applied pressures. The total DOS at E_F for the majority spin is about 25 times larger than that for the minority spin for all pressures. The DOS is dominated by two contributions for both spins. The peak well below the Fermi energy (E_F) originates essentially from the metallic full d shell whereas the spike around E_F is due to the Pr 4f states for the majority spin. Other contributions are much smaller on this scale and come from the d and s states of Pr and the p and s states of Ag. At the highest

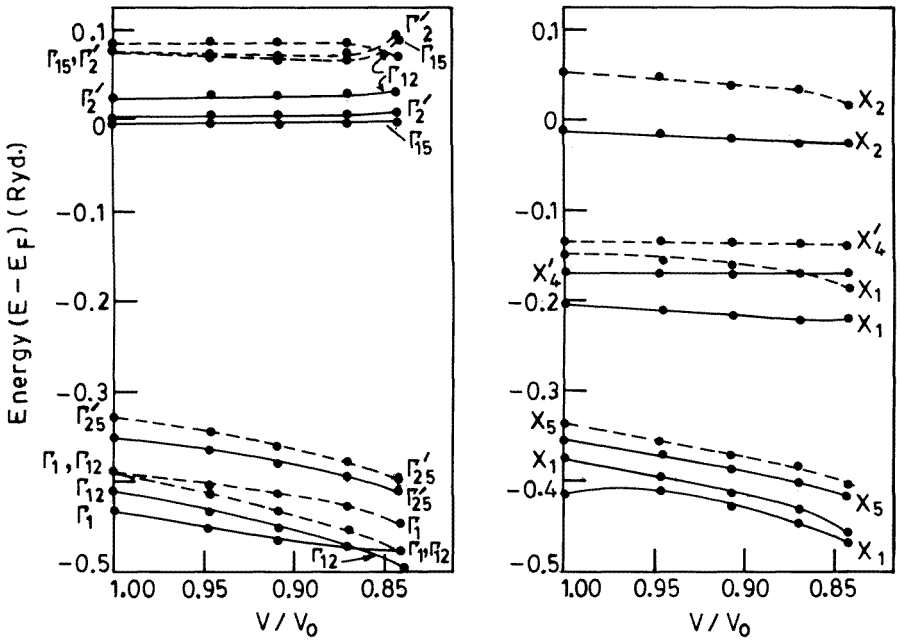

Figure 3. The behaviour of the eigenvalues for the majority (——) and for the minority (– – –) spins at Γ and X points under pressure.

pressure, corresponding to a lattice constant $a_1 = 3.50$ Å, the Fermi energy is 0.617 Ryd whereas that at the experimental lattice constant $a = 3.718$ Å is 0.476 Ryd. Thus the Fermi energy increases with the application of pressure. The peak well below the Fermi energy shifts towards lower energy and becomes flattened for both spins whereas the spike around E_F for the majority spin more or less remains fixed under pressure. A small peak about 0.25 Ryd below E_F originating from d states of Pr shifts slightly towards lower energy and its DOS increases for both spins with applied pressure. The peaks and structures above E_F are mainly derived from the d states of Pr, as is evident from the partial DOS shown in figure 5.

The angular-momentum-decomposed DOS at E_F, $N_1(E_F)$ and the corresponding charges, n_1, inside the Wigner–Seitz spheres are shown in table 2. From table 2 it can be seen that the maximum contribution to $N_1(E_F)$ originates from Pr f states and other considerable contributions come from Pr d and Ag p states, indicating a hybridization among them near E_F. Such hybridization is in agreement with the appearance of f and d states of Pr and p states of Ag in the same energy range near E_F, as can be seen from figure 5. The number of d electrons of Ag decreases from 9.573 to 9.394 while that of the p electrons increases from 0.717 to 0.814 with increasing pressure. The number of f electrons of Pr decreases from 2.303 to 2.243 but the number of d electrons increases from 1.400 to 1.579 under pressure. Thus the number of f electrons remains almost constant with pressure. However, the number of electrons at a particular site depends on the size of the sphere surrounding each lattice site. So, table 2 gives only a comparative trend of the volume-dependence of the occupation number.

The magnetic moment, μ, calculated by integrating the majority and minority spin components up to E_F for each volume is summarized in table 3. It is evident that the main

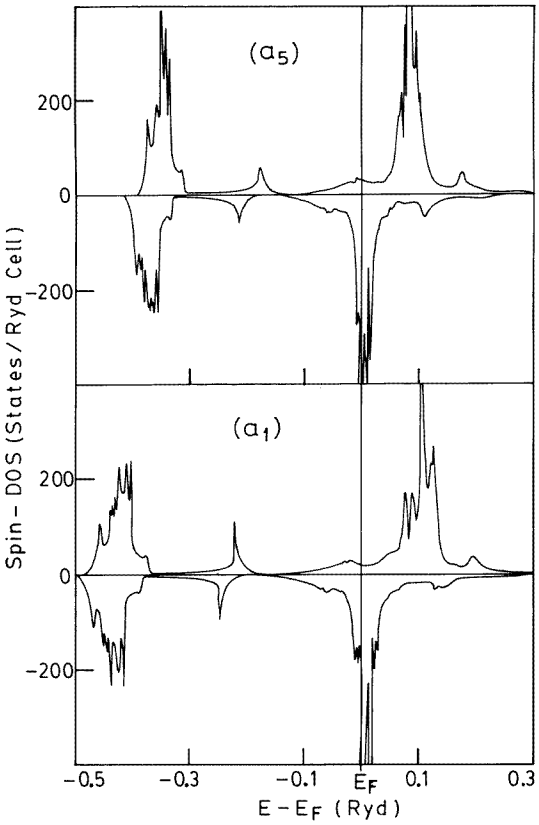

Figure 4. Total densities of states (DOSs) for both spins at ambient (upper graph) and applied pressure (lower graph). The upper graph in each panel is for minority spins and the lower graph is for majority spins.

contributions to the magnetic moment arises from the f states of Pr for all lattice constants, indicating that the f electrons play a significant role in the magnetic properties. The larger value of μ in comparison with that for CeAg is due to the additional f electron in Pr. As a result, E_F moves towards the huge peak in the majority DOS as shown in figure 4. This leads to a very high contribution from the majority component which is not balanced by the minority DOS. This is in agreement with the results of partial occupation number n_1 in table 2 and shows that the number of f electrons for the majority spin is about ten times greater than that for the minority spin. The behaviour of the magnetic moment versus volume reduction is shown in figure 6. We have plotted $\mu_T(a)/\mu_T(a_0)$ as a function of a/a_0, where a and a_0 are the lattice constants at applied and normal pressures, respectively, and $\mu_T(a)$ represents the total magnetic moment at a given lattice constant a. The magnetic moment decreases with reduced volume, as shown in figure 6. The moment reduction may be due to the f electron delocalization under pressure. From table 2 we observe that n_f changes from 2.303 to 2.243 on going from ambient to high pressure. Thus there is no significant delocalization of f electrons by volume reduction. The moment reduction may be due to the weaker exchange interaction between f up and down spin components.

For PrAg the value of T_C increases between 0 and 5 kbar, then drops to zero at about 17 kbar [8] which indicates the instability of the FM ground state phase at high pressure.

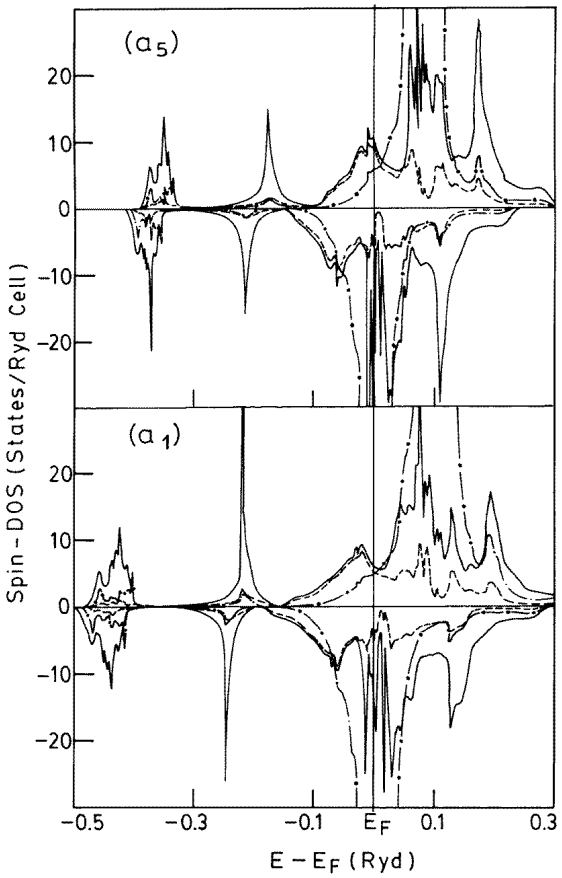

Figure 5. Partial densities of states for d (——) and f (— · —) components of Pr and for the p (– – –) component of Ag for both spins at ambient (upper graph) and applied pressure (lower graph). The upper graph in each panel is for minority spins and the lower graph is for majority spins.

In order to study the stability of the FM phase we calculated the total energy at different reduced lattice constants, as shown in figure 7. The calculated total energies were fitted to Murnaghan's equation of state [27] and the best fitted results yielded the equilibrium lattice constant $a_0 = 3.66$ Å and the bulk modulus $B_0 = 375.6$ kbar. The calculated pressure corresponding to a_0 is about 26 kbar. Thus the FM phase is stable up to 26 kbar which is very close to the experimental value 17 kbar.

4. Conclusion

Extensive electronic structure calculations with different reduced lattice constants were performed to study the ground state properties of the FM phase of PrAg, which was calculated to be stable up to 26 kbar, slightly greater than the experimental value of 17 kbar. The difference may be due to our having neglected the tetragonal distortion which is observed in PrAg at high pressure. Our calculations show that the f states mainly hybridize with the extended Pr d and Ag p states near E_F. From the spin-polarized calculation

Table 2. Angular-momentum-decomposed DOSs at E_F, $N_1(E_F)$, and charge, n_1, within the Wigner–Seitz spheres for PrAg in the ferromagnetic cubic phase at different lattice constants. ↑ and ↓ represent majority and minority spins respectively.

			Pr				Ag				
			s	p	d	f	s	p	d	f	Total
$N_1(E_F)$	a_1	↑	0.533	0.948	11.948	202.880	0.268	2.461	0.030	1.207	220.275
		↓	0.638	0.533	2.950	2.350	0.245	2.585	0.267	0.053	9.619
	a_2	↑	0.886	0.798	14.743	266.810	0.316	3.609	0.025	1.602	288.789
		↓	0.851	0.579	3.419	3.994	0.263	3.160	0.189	0.056	12.511
	a_3	↑	0.792	1.180	18.368	316.667	0.300	3.085	0.322	1.671	342.385
		↓	1.043	0.670	3.959	3.549	0.277	3.533	0.178	0.053	13.262
	a_4	↑	0.733	0.912	13.717	285.695	0.273	2.637	0.243	1.376	305.586
		↓	1.343	0.799	4.664	3.271	0.301	4.123	0.170	0.055	14.726
	a_5	↑	0.742	0.834	14.422	357.091	0.259	2.745	0.207	1.418	377.718
		↓	1.571	1.021	5.188	2.712	0.311	4.495	0.152	0.052	15.502
n_1	a_1	↑	0.247	0.229	0.891	2.043	0.505	0.454	4.698	0.029	9.096
		↓	0.234	0.200	0.688	0.200	0.509	0.360	4.696	0.011	6.898
	a_2	↑	0.254	0.236	0.899	2.029	0.507	0.455	4.729	0.028	9.137
		↓	0.229	0.195	0.643	0.226	0.512	0.337	4.710	0.010	6.862
	a_3	↑	0.260	0.242	0.884	2.071	0.506	0.448	4.749	0.025	9.185
		↓	0.232	0.197	0.622	0.198	0.512	0.323	4.719	0.009	6.812
	a_4	↑	0.264	0.245	0.858	2.108	0.509	0.443	4.794	0.023	9.244
		↓	0.231	0.197	0.596	0.174	0.514	0.307	4.728	0.008	6.755
	a_5	↑	0.272	0.253	0.838	2.158	0.509	0.433	4.822	0.020	9.316
		↓	0.232	0.198	0.562	0.145	0.514	0.284	4.740	0.007	6.682

Table 3. Angular-momentum-decomposed magnetic moment, μ_1, and total magnetic moment, μ_T, in Bohr magnetons in the ferromagnetic cubic phase at different lattice constants.

	Pr				Ag				
	s	p	d	f	s	p	d	f	Total
a_1	0.013	0.028	0.203	1.842	−0.004	0.094	0.002	0.018	2.196
a_2	0.024	0.041	0.256	1.802	−0.005	0.118	0.019	0.018	2.273
a_3	0.028	0.045	0.262	1.872	−0.005	0.125	0.030	0.016	2.378
a_4	0.033	0.048	0.262	1.935	−0.004	0.136	0.066	0.015	2.491
a_5	0.040	0.055	0.276	2.012	−0.004	0.150	0.093	0.013	2.635

we obtained that the magnetic moment decreases under pressure. The contribution from f states to the magnetic moment was about 84% for all pressures. We also found that the f states were localized throughout the pressure range studied while the variation of the electronic density of states with volume affected the stability of magnetic phase. This supported the hypothesis of the magnetic RKKY interaction and the Kondo compensation of the magnetic moment. The one-electron LSDA calculations alone cannot be conclusive about the presence of the Kondo effect, which is a many-body phenomenon, but they provide a basic framework for understanding the competition between the RKKY and Kondo effects. We, therefore, conclude that, although the one-electron LSDA calculations yielded

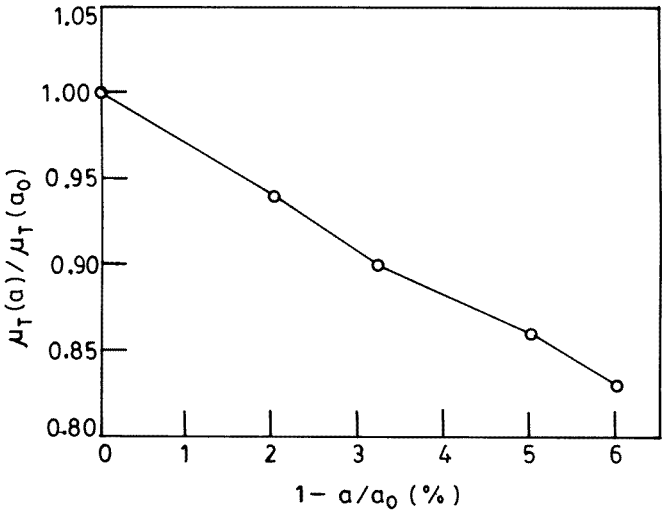

Figure 6. A plot of $\mu_T(a)/\mu_T(a_0)$ as a function of a/a_0. The line connecting the calculated values is drawn as a guide for the eyes only.

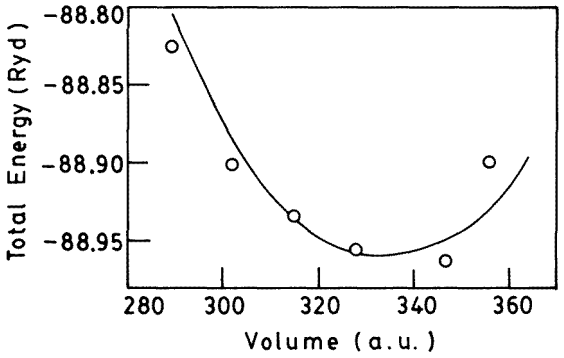

Figure 7. The total energy versus volume for the ferromagnetic phase in PrAg. The small circles denote the calculated values and the curve is Murnaghan's equation of state fitted to the calculated results.

a decrease in the magnetic moment, it is not sufficient to cause the observed instability, so that many-body effects must be invoked.

Acknowledgment

P K Sinharoy acknowledges support received from the University Grants Commission, New Delhi, Government of India.

References

[1] Schmitt D, Morin P and Pierre J 1978 *J. Magn. Magn. Mater.* **8** 249
[2] Takke R, Dolezal N, Assmsus W and Luthi B 1981 *J. Magn. Magn. Mater.* **23** 247

[3] Morin P, Rouchy J, Miyako Y and Nishioka T 1988 *J. Magn. Magn. Mater.* **76–77** 319
Hyomi K, Amitsuka H, Nishioka T, Murayama S, Miyako Y, Nishiyama K, Nagamine K, Yamazaki T and Morin P 1988 *J. Magn. Magn. Mater.* **76–77** 462
[4] Morin P 1988 *J. Magn. Magn. Mater.* **71** 151
[5] Kurisu K, Kadomatsu H and Fujiwara H 1983 *J. Phys. Soc. Japan* **52** 4349
[6] Brun T O, Kouvel J S and Lander G H 1976 *Phys. Rev.* B **13** 5007
[7] Morin P and Schmitt D 1982 *Phys. Rev.* B **26** 3891
[8] Kadomatsu H, Kurisu M and Fujiwara H 1984 *J. Phys. Soc. Japan* **53** 1819
[9] Canepa F, Merlo F and Palenzona A 1989 *J. Phys.: Condens. Matter* **1** 1429
[10] Kurisu M 1987 *J. Phys. Soc. Japan* **56** 4064
[11] Kurisu M, Kadomatsu H, Fujiwara H, Ohyama T, Sakurai J and Komura Y 1987 *J. Phys. Soc. Japan* **56** 3240
[12] Kadomatsu H, Kurisu M and Fujiwara H 1987 *J. Phys. F: Met. Phys.* **17** L305
[13] Buschow K H J, de Jong J P, Zandbergen H W and van Laar B 1975 *J. Appl. Phys.* **46** 1352
[14] Ihrig H and Methfessel S 1976 *Z. Phys.* B **24** 385
[15] Steglich F, Ahlheim U, Bredl C D, Geibel C, Grauel A, Lang M, Sparn G, Krimmel A, Loidl A and Assmsus W 1992 *J. Magn. Magn. Mater.* **108** 5
[16] Doniach S 1977 *Physica* B **91** 231
[17] Continenza A and Monachesi P 1992 *Phys. Rev.* B **46** 6217
Monachesi P and Continenza A 1993 *Phys. Rev.* B **47** 14 622
[18] Fujita T, Suzuki T, Nishigori S, Takabatake T, Fujii H and Sakurai J 1992 *J. Magn. Magn. Mater.* **108** 35
[19] Kittel C 1963 *Quantum Theory of Solids* (New York: Wiley)
[20] Kondo J 1969 *Solid State Physics* vol 23, ed H Ehrenreich *et al* (New York: Academic) p 183
[21] Umehara M and Kasuya T 1976 *J. Phys. Soc. Japan* **40** 13
[22] Slater J C 1960 *Quantum Theory of Atomic Structure* vol 1 (New York: McGraw-Hill) p 245
[23] Andersen O K 1975 *Phys. Rev.* B **12** 3060
[24] Skriver H L 1984 *The LMTO Method* (Berlin: Springer)
[25] von Barth U and Hedin L 1972 *J. Phys. C: Solid State Phys.* **5** 1629
[26] Lehman G and Taut M 1972 *Phys. Status Solidi* b **54** 469
[27] Murnaghan F D 1944 *Proc. Natl. Acad. Sci. USA* **30** 244